Optics Letters

Coherent solid-state LIDAR with silicon photonic optical phased arrays

Christopher V. Poulton,[1,2,*] Ami Yaacobi,[1] David B. Cole,[1] Matthew J. Byrd,[1,2] Manan Raval,[1] Diedrik Vermeulen,[1,2] and Michael R. Watts[1]

[1]Research Laboratory of Electronics, Massachusetts Institute of Technology, Cambridge, Massachusetts 02139, USA
[2]Current affiliation is Analog Photonics, One Marina Park Drive, Boston, Massachusetts 02210, USA
*Corresponding author: cpoulton@mit.edu

Received 22 June 2017; revised 12 September 2017; accepted 12 September 2017; posted 12 September 2017 (Doc. ID 300540); published 5 October 2017

We present, to the best of our knowledge, the first demonstration of coherent solid-state light detection and ranging (LIDAR) using optical phased arrays in a silicon photonics platform. An integrated transmitting and receiving frequency-modulated continuous-wave circuit was initially developed and tested to confirm on-chip ranging. Simultaneous distance and velocity measurements were performed using triangular frequency modulation. Transmitting and receiving optical phased arrays were added to the system for on-chip beam collimation, and solid-state beam steering and ranging measurements using this system are shown. A cascaded optical phase shifter architecture with multiple groups was used to simplify system control and allow for a compact packaged device. This system was fabricated within a 300 mm wafer CMOS-compatible platform and paves the way for disruptive low-cost and compact LIDAR on-chip technology.

OCIS codes: (130.3120) Integrated optics devices; (110.5100) Phased-array imaging systems; (280.3640) Lidar.

https://doi.org/10.1364/OL.42.004091

Light detection and ranging (LIDAR) has garnered significant interest as a ranging technology because of its potential to achieve long range and high resolution. These advantages arise from the fact that optical wavelengths afford smaller diffraction angles for a given aperture size than microwave-based radar systems. LIDAR has seen extensive use in autonomous vehicles [1], robotics [2], aerial mapping [3], and atmospheric measurements [4]. Autonomous systems are a key market for LIDAR devices and normally require beam steering or a form of flash illumination [5] in order to map the surrounding environment. Flash illumination puts a considerable burden on system requirements by necessitating a high peak laser power. Therefore, many LIDAR systems available today utilize a mechanical mechanism for beam steering such as a gimbal. However, such mechanisms limit the scan rate, decrease reliability, and increase the system cost. Recently, there has been an emphasis towards solid-state beam steering systems [6] to increase system durability.

Integrated photonics provide a path for low-cost chip-scale LIDAR systems. Silicon photonics, in particular, offer a low-cost technology that can be integrated with CMOS electronics [7] and lasers [8]. Since they may be fabricated on 300 mm silicon wafers, silicon photonic devices can be produced at a high volume in CMOS foundries. Integrated optical phased arrays have been extensively researched in recent years due to their capability of solid-state beam steering [9–18]. Recent demonstrations of optical phased arrays have shown a large aperture size of 4×4 mm^2 [16], a potential fast scanning rate up to 200 MHz [17], and a high steering range of 80° [18], which are promising developments for on-chip LIDAR.

In this Letter, we present, to the best of our knowledge, the first demonstration of coherent LIDAR with integrated optical phased arrays for solid-state beam steering. Frequency-modulated continuous-wave (FMCW) LIDAR is utilized with a compact laser diode. In an integrated setting, FMCW LIDAR [19] reduces system complexity compared to time-of-flight detection because avalanche photodiodes are not required due to the coherent amplification, and low-cost laser sources are available. Furthermore, FMCW LIDAR also allows for simultaneous Doppler-based velocity measurements at no additional cost or complexity. First, a FMCW photonic circuit was created consisting of an on-chip balanced photodetector with transmitting and receiving edge couplers and tested with a bulk optics collimation lens. Target distance and velocity measurements are shown with this circuit. Next, an optical phased array was designed and characterized with a steering range of $46° \times 36°$. Finally, this optical phased array is added as a transmitter (TX) and receiver (RX) to the FMCW circuit to allow for a chip-scale lens-free LIDAR system. Solid-state steering is performed while ranging measurements are demonstrated.

FMCW detection is commonly used in RADAR systems [20] and was chosen to minimize the cost of a silicon-based chip-scale LIDAR system. The use of silicon is desirable due to its CMOS compatibility and the capability to realize compact and efficient optical phase shifters with either the thermo-optic or the plasma dispersion effect. However, due to the

transparency window of silicon, wavelengths above ~1100 nm must be used. Therefore, pulsed sources and detectors at 905 nm seen in many LIDAR systems today cannot be used in a silicon photonic system. Wavelengths around 1550 nm are commonly used in telecom devices and continuous-wave sources are available at a low cost. This wavelength band also has the benefits of low atmospheric absorption and eye-safety at high power levels. It is also simple to perform slight optical frequency chirps on DFB lasers by injection current modulation so electronic-based frequency sweeping methods are not needed. However, it is important to note that the laser coherence length puts an upper bound on the target distance in FMCW detection.

The concept of FMCW LIDAR with triangular modulation is illustrated in Fig. 1(a) [19]. Triangular modulation is utilized to help resolve the distance/velocity ambiguity caused by an induced Doppler shift from a moving target. Using coherent detection, a time delay, Δt, between a frequency-modulated optical received signal (RX) and a local oscillator (LO) will create an electrical beat frequency. For a stationary target, a single beat frequency, f_{Dis}, which is proportional to the target distance is observed. This frequency is given by $f_{\mathrm{Dis}} = \Delta t\hat{s} = \frac{2R}{c}\hat{s}$, where $\hat{s}$ is the linear sweep rate of the laser, R is the distance to the target, and c is the speed of light. For a moving target, two distinct beat frequencies occur due to the Doppler shift on the RX signal. These two beat frequencies, f_{IF1} and f_{IF2}, occur in different time regions, depending on the direction of the laser frequency sweep. The difference of the two beat frequencies is twice the induced Doppler shift, $f_{\mathrm{IF1}} - f_{\mathrm{IF2}} = 2f_{\mathrm{Doppler}} \approx 2\frac{vf_0}{c}$, where v is the velocity of the target and f_0 is the frequency of the input light. The average of the two beat frequencies is proportional to the time-of-flight distance to the target, $\frac{f_{\mathrm{IF1}}+f_{\mathrm{IF2}}}{2} = f_{\mathrm{Dis}}$. By detecting both beat frequencies, simultaneous distance and velocity measurements can be performed.

A photonic circuit was used to test on-chip FMCW LIDAR, and is illustrated in Fig. 1(b). It was fabricated using 193 nm immersion lithography on a 220 nm thick silicon-on-insulator wafer with 2 μm of buried oxide. The optical input is coupled using a silicon inverse taper edge coupler and a split with a 3 dB adiabatic coupler to act as an LO and a TX. The TX signal is coupled off the side of the chip with an edge coupler. Due to the small aperture of the edge coupler, an off-chip collimating lens is required. After collimation, the TX light is incident on a target. The light reflected off the target is received through another edge coupler and coherently beaten against the LO, which is detected with an on-chip balanced germanium photodetector. An external transimpedance amplifier is used to convert the photocurrent to a voltage that is analyzed by an oscilloscope. The experiments were carried out with a cube-reflector target placed on a 1.5 m long motorized stage with speed control up to 300 mm/s (AeroTech Pro225-HS). The light was input to the chip using a cleaved SMF-28 fiber and the TX/RX light was collimated with a 20× objective.

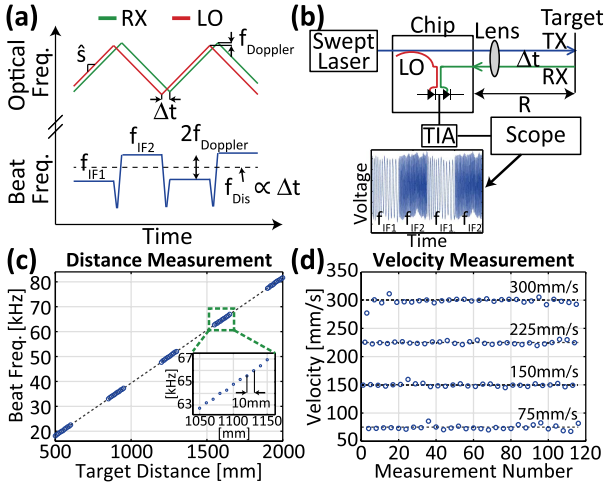

Fig. 1. (a) Concept of FMCW LIDAR with triangular modulation. (b) Silicon photonic LIDAR circuit with collimating lens. (c) Measured beat frequency at various stationary target distances at 10 mm intervals. (d) Velocity measurements on a moving target at different distances.

Optical frequency modulation was achieved by modulating the injection current of a compact DFB laser diode (JDSU CQF935 Series). Current modulation was performed with an arbitrary function generator with a driving function designed for a linear triangular optical frequency sweep. Further closed loop linearization could be achieved with an auxiliary optical delay line [21,22]. Measurements were taken on a stationary target at varying known distances at 10 mm intervals. For this experiment, the frequency of the laser injection current waveform was 100 Hz, resulting in a linear optical frequency sweep rate of 6.4 THz/s. The target distance ranged from 0.5 to 2.0 m, and Fig. 1(c) shows the measured beat frequency at each distance. The absolute errors were less than 10 mm for distances up to 2 m, showing a noise-limited resolution of 20 mm. LIDAR measurements were then taken on a moving target at various speeds and distances to test simultaneous distance and velocity measurements. The four velocities measured were 75, 150, 225, and 300 mm/s at distances ranging from 0.5 to 2.0 m. In this experiment, the injection current waveform frequency was increased to 5 kHz to increase the laser sweep rate to 190 THz/s. This was done to ensure that the induced Doppler frequency was less than the stationary target beat frequency (at the cost of some sweep nonlinearities). The velocity measurements are shown in Fig. 1(d) and show good agreement with the motion track velocity. For this optical sweep rate and a 2 m range, homodyne detection has an unambiguous target velocity of $v = \frac{2R\hat{s}}{f_0} = 3.93$ m/s. A photonic circuit allowing for heterodyne detection could also be used for an unambiguous detection of the Doppler shift.

The system in Fig. 1 requires a lens to have an adequate small beam divergence angle. Integrated optical phased arrays can replace the edge couplers in order to emit out-of-plane with a small divergence angle and receive with a large collection area. Assuming that the entire transmitted beam hits an isotropically scattering target, the power received is

$$P_{\mathrm{RX}} = P_{\mathrm{In}}\eta_{\mathrm{TX}}\frac{\rho A_{\mathrm{RX}}}{4\pi R^2}\eta_{\mathrm{RX}}, \tag{1}$$

where P_{RX} is the received power, P_{In} is the input power, η_{TX} is the efficiency of the TX, ρ is the reflectivity of the target, A_{RX} is the RX area, R is the distance to the target, and η_{RX} is the efficiency of the RX. Equation (1) shows that a large RX aperture is needed in order to overcome the R^2 dependence of the received power. Due to on-chip losses occurring within both the TX and RX array, η_{TX} and η_{RX}, it is also crucial to have loss-low phase shifters and high side lobe suppression.

Figure 2(a) shows a 3D rendering of the optical phased array designed for a solid-state LIDAR system. SEMs of the fabricated device are shown in Figs. 2(b)–2(d). The phased array consists of 50 grating-based antennas placed at a 2 μm pitch which theoretically forms a main beam full-width at half-maximum (FWHM) intensity spot size of 0.80° in the array dimension and grating lobes at ±51° when the main beam is centered at 0°. The antenna length is 500 μm and is designed to have a uniform emission pattern which predicts a 0.16° FWHM spot size in the antenna dimension. The antennas are formed by apodized periodic fully etched perturbations on the side of a silicon waveguide. A full etch is used instead of a ridge etch to minimize the risk of over or under etching. Silicon nitride overlays [9,10] can also be used to reduce this risk. Here, the perturbation value and period are apodized from 7 and 701 nm to 43 and 759 nm.

A grouped cascaded phase shifter architecture is utilized to apply phase shifts to antenna elements. The light to each antenna is evanescently coupled from a common bus waveguide. The cascaded evanescent couplers have a constant 120 nm coupling gap and coupling lengths that increase by 1.89 μm to create a uniform amplitude distribution. A waveguide-embedded thermal phase shifter is placed between each coupler. Each phase shifter has a resistance of 5.7 kΩ and produces a 2π phase shift at 12 V, resulting in a 13 mW/π efficiency. Unlike previous work [11], the cascaded phase shifters are grouped into three distinct electrical signals in order to achieve fine tuning of the beam to account for any fabrication-induced phase noise. For beam steering applications, grouped cascaded phase shifters allow for a linear phase ramp in element phase distribution without complex individual element phase control, simplifying control for large element counts.

Figure 2(e) shows the output of the phased array when an infrared (IR) card is placed above it. A strong main beam and grating lobe is clearly visible. Another grating lobe on the other side of the main lobe is not captured by the card. The grating lobes have similar power to the main beam because of imperfections in the design of the element factor, which can be mitigated by appropriately altering the antenna design. Despite strong grating lobes, the power in the main beam was measured to be 1 mW, limited by the laser input power and the nonlinearities of silicon. Intensity cross sections of the far field are shown in Fig. 2(f). The far-field FWHM spot size of the beam is measured to be 0.85° × 0.18°, which is in good agreement with the theoretical value of 0.80° × 0.16°, with a side lobe suppression of about 8 dB. Figure 2(g) shows the far field of the device when steered using thermal and wavelength tuning. Thermal tuning only steers in the array dimension, ϕ. Wavelength tuning primarily steers in the antenna dimension, θ, but also steers slightly in ϕ because of the inherent optical path length addition in the cascaded phase shifters. A total steering range of 46° × 36° was achieved with thermal steering, which consumed up to 1.2 W of electrical power, and wavelength tuning from 1454 to 1641 nm (Keysight 81606A).

Utilizing the phased array shown in Fig. 2, a LIDAR system was created using a TX and RX phased array. A schematic of this system is shown in Fig. 3(a). It is similar to Fig. 1(a), but is lens-free due to the beam collimation capability of the phased array and can perform solid-state steering. To give a sense of the size of this LIDAR system, Fig. 3(b) shows the 6 mm × 0.5 mm LIDAR chiplet on top of a dime and Fig. 3(c) shows an optical micrograph. Here, the tap from the input waveguide to realize the LO was achieved with a 10% directional

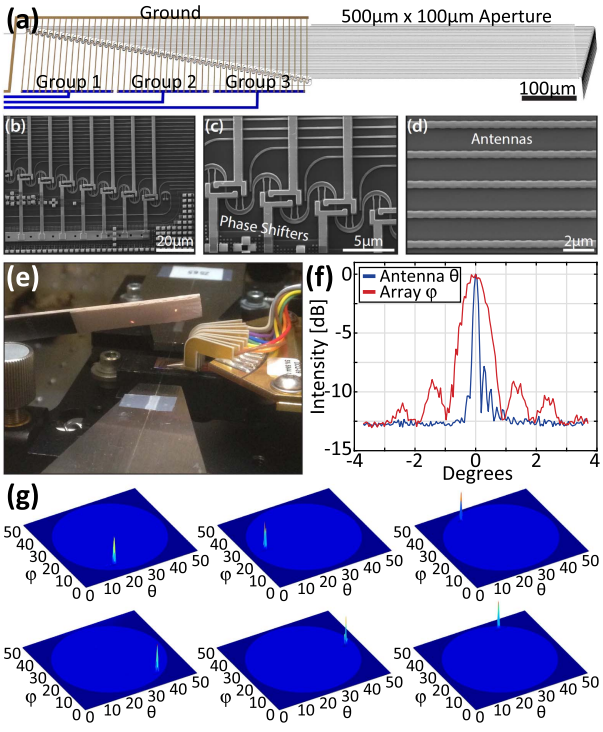

Fig. 2. (a) 3D rendering of the optical phased array with (b)–(d) SEM images. (e) Main beam and grating lobe output of the array seen with an IR card. (f) Intensity cross sections of the far-field spot. (g) Far field of the array at different thermal and wavelength tuning values.

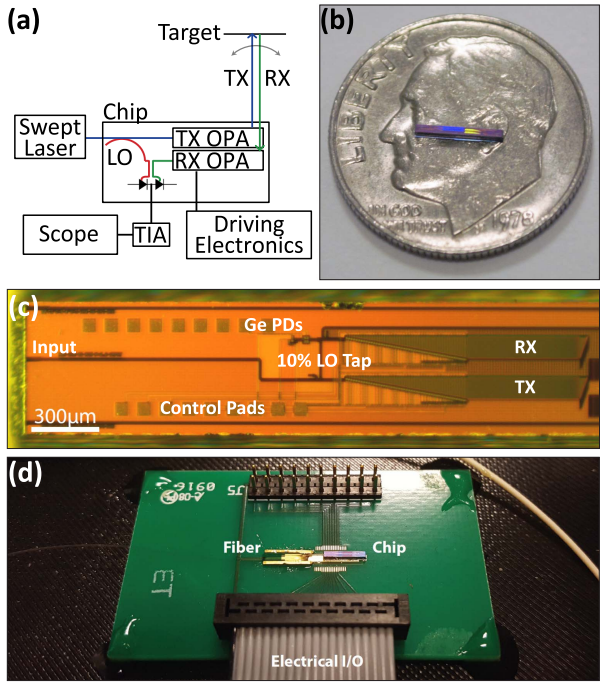

Fig. 3. (a) Schematic of the solid-state LIDAR system with transmitting and receiving optical phased arrays. (b) Chiplet containing LIDAR system on top of a dime. (c) Optical micrograph of the device. (d) Packaged system with epoxied fiber.

coupler. This value was chosen to ensure that the LO did not saturate the balanced photodetector. Furthermore, the germanium photodetector design was improved by using a mode-evolution-based coupler [23] with a 4 μm × 12 μm germanium size. The system is controlled using nine copper electrical pads: three for the TX array, three for the RX array, two for the signal and bias of the balanced photodetector, and one for ground. The chiplet was packaged in a chip-on-board configuration with an epoxied fiber, as shown in Fig. 3(d).

In order to test the steered LIDAR operation of the device, three targets were placed at different incident angles from the chip, as shown in Fig. 4(a). The targets were created with reflective tape. By steering the transmitting and receiving phased arrays simultaneously, each of the targets was measured separately. The distance to each target is shown in Fig. 4(b), and the raw data from the photodetector are shown in Fig. 4(c). A frequency component proportional to the target distance is observed in the raw data. No noticeable crosstalk between targets was measured, indicating that the beam was confined to be incident on a single target. Unfortunately, the angle range shown, about 20°, was near the limit that could be measured due to thermal crosstalk between the phase shifters and the balanced photodetector. Future iterations will ensure that the photodetectors are thermally isolated from the phased arrays or use electro-optic phase shifters.

In conclusion, we have demonstrated coherent LIDAR on a silicon photonics chip using optical phased arrays for solid-state beam steering for the first time, to the best of our knowledge. Coherent detection utilizes an on-chip LO for amplification which allows for the use of standard germanium photodetectors. The initial system shown employed FMCW LIDAR with triangular frequency modulation and achieved simultaneous distance and velocity measurements with a 2 m range and a resolution of 20 mm. Frequency modulation was realized by modulating the injection current of an off-chip compact laser diode. After the demonstration of this system, optical phased arrays were added as a TX and RX within the FMCW LIDAR photonic circuit. The optical phased arrays utilized a grouped cascaded phase shifter architecture for simple control. The beam was steered to three targets, and their distances were measured up to 0.5 m. In this Letter, the maximum range and target diffusivity were limited by the aperture size of the phased array, which can easily be scaled as shown in [16]. The work shown in this Letter paves the way for on-chip LIDAR systems based on optical phased arrays with the ultimate application of a centimeter-scale low-cost autonomous vehicle LIDAR.

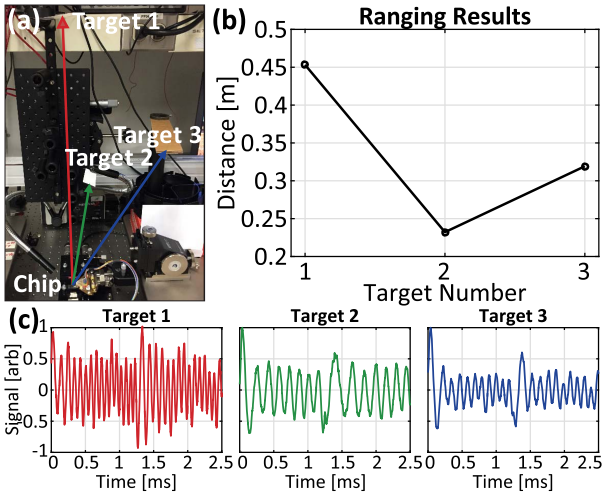

Fig. 4. (a) Image of targets in the laboratory placed at different angles from the chip. (b) Ranging results of each target. (c) Raw photodetector data for each target.

Funding. Defense Advanced Research Projects Agency (DARPA) (HR0011-12-2-0007).

Acknowledgment. The authors thank Dr. Joshua Conway for helpful discussions.

REFERENCES

1. J. Levinson, J. Askeland, J. Becker, J. Dolson, D. Held, S. Kammel, J. Z. Kolter, D. Langer, O. Pink, V. Pratt, M. Sokolsky, G. Stanek, D. Stavens, A. Teichman, M. Werling, and S. Thrun, *Intelligent Vehicles Symposium (IV)* (IEEE, 2011) pp. 163–168.
2. J. Lalonde, N. Vandapel, D. Huber, and M. Hebert, J. Field Robot. **23**, 839 (2006).
3. Y. Lin, J. Hyyppa, and A. Jaakkola, IEEE Geosci. Remote Sens. Lett. **8**, 426 (2011).
4. J. Schween, A. Hirsikko, U. Löhnert, and S. Crewell, Atmos. Meas. Tech. **7**, 3685 (2014).
5. M. A. Albota, B. F. Aull, D. G. Fouche, R. M. Heinrichs, D. G. Kocher, R. M. Marino, J. G. Mooney, N. R. Newbury, M. E. O'Brien, B. E. Player, B. C. Willard, and J. J. Zayhowski, Lincoln Lab. J. **13**, 351 (2002).
6. S. R. Davis, S. D. Rommel, D. Gann, B. Luey, J. D. Gamble, M. Ziemkiewicz, and M. Anderson, Proc. SPIE **9832**, 98320K (2016).
7. C. Sun, M. T. Wade, Y. Lee, J. S. Orcutt, L. Alloatti, M. S. Georgas, A. S. Waterman, J. M. Shainline, R. R. Avizienis, S. Lin, B. R. Moss, R. Kumar, F. Pavanello, A. H. Atabaki, H. M. Cook, A. J. Ou, J. C. Leu, Y.-H. Chen, K. Asanovic, R. J. Ram, M. A. Popovic, and V. M. Stojanovic, Nature **528**, 534 (2015).
8. A. Y. Liu, C. Zhang, J. Norman, A. Snyder, D. Lubyshev, J. M. Fastenau, A. W. Liu, A. C. Gossard, and J. E. Bowers, Appl. Phys. Lett. **104**, 041104 (2014).
9. M. Zadka, Y.-C. Chang, A. Mohanty, C. Phare, S. P. Roberts, and M. Lipson, *Conference on Lasers and Electro-Optics* (Optical Society of America, 2017), paper STh1M.6.
10. K. Shang, C. Qin, Y. Zhang, G. Liu, X. Xiao, S. Feng, and S. B. Yoo, Opt. Express **25**, 19655 (2017).
11. A. Yaacobi, J. Sun, M. Moresco, G. Leake, D. Coolbaugh, and M. R. Watts, Opt. Lett. **39**, 4575 (2014).
12. J. Hulme, J. Doylend, M. Heck, J. Peters, M. Davenport, J. Bovington, L. Coldren, and J. Bowers, Opt. Express **23**, 5861 (2015).
13. H. Abediasl and H. Hashemi, Opt. Express **23**, 6509 (2015).
14. T. Komljenovic, R. Helkey, L. Coldren, and J. E. Bowers, Opt. Express **25**, 2511 (2017).
15. S. Chung, H. Abediasl, and H. Hashemi, IEEE International Solid-State Circuits Conference (ISSCC) (2017), pp. 262–263.
16. C. V. Poulton, M. J. Byrd, M. Raval, Z. Su, N. Li, E. Timurdogan, D. Coolbaugh, D. Vermeulen, and M. R. Watts, Opt. Lett. **42**, 21 (2017).
17. F. Aflatouni, B. Abiri, A. Rekhi, and A. Hajimiri, Opt. Express **23**, 21012 (2015).
18. D. N. Hutchison, J. Sun, J. K. Doylend, R. Kumar, J. Heck, W. Kim, C. T. Phare, A. Feshali, and H. Rong, Optica **3**, 887 (2016).
19. D. Pierrottet, F. Amzajerdian, L. Petway, B. Barnes, G. Lockard, and M. Rubio, MRS Proc. **1076**, 1076 (2008).
20. A. G. Stove, IEE Proc. F Radar Signal Process. **139**, 343 (1992).
21. N. Satyan, A. Vasilyev, G. Rakuljic, V. Leyva, and A. Yariv, Opt. Express **17**, 15991 (2009).
22. B. Behroozpour, P. A. Sandborn, N. Quack, T.-J. Seok, Y. Matsui, M. C. Wu, and B. E. Boser, IEEE J. Solid-State Circuits **52**, 161 (2017).
23. M. J. Byrd, E. Timurdogan, Z. Su, C. V. Poulton, N. M. Fahrenkopf, G. Leake, D. D. Coolbaugh, and M. R. Watts, Opt. Lett. **42**, 851 (2017).